PNAS RESEARCH ARTICLE | BIOCHEMISTRY

Spns1 is a lysophospholipid transporter mediating lysosomal phospholipid salvage

Menglan He[a,1], Alvin C. Y. Kuk[a,1], Mei Ding[b,c], Cheen Fei Chin[a], Dwight L.A. Galam[a], Jie Min Nah[a], Bryan C. Tan[a], Hui Li Yeo[d], Geok Lin Chua[a], Peter I. Benke[b,c], Markus R. Wenk[b,c], Lena Ho[a,d,e], Federico Torta[b,c,2], and David L. Silver[a,2]

Edited by Stephen Young, University of California Los Angeles David Geffen School of Medicine, Los Angeles, CA; received June 17, 2022; accepted August 28, 2022

The lysosome is central to the degradation of proteins, carbohydrates, and lipids and their salvage back to the cytosol for reutilization. Lysosomal transporters for amino acids, sugars, and cholesterol have been identified, and the metabolic fates of these molecules in the cytoplasm have been elucidated. Remarkably, it is not known whether lysosomal salvage exists for glycerophospholipids, the major constituents of cellular membranes. By using a transport assay screen against orphan lysosomal transporters, we identified the major facilitator superfamily protein Spns1 that is ubiquitously expressed in all tissues as a proton-dependent lysophosphatidylcholine (LPC) and lysophosphatidylethanolamine (LPE) transporter, with LPC and LPE being the lysosomal breakdown products of the most abundant eukaryotic phospholipids, phosphatidylcholine and phosphatidylethanolamine, respectively. Spns1 deficiency in cells, zebrafish embryos, and mouse liver resulted in lysosomal accumulation of LPC and LPE species with pathological consequences on lysosomal function. Flux analysis using stable isotope-labeled phospholipid apolipoprotein E nanodiscs targeted to lysosomes showed that LPC was transported out of lysosomes in an Spns1-dependent manner and re-esterified back into the cytoplasmic pools of phosphatidylcholine. Our findings identify a phospholipid salvage pathway from lysosomes to the cytosol that is dependent on Spns1 and critical for maintaining normal lysosomal function.

phospholipid | transporter | Mfsd2a | autophagy | lysosome

The lysosome is an acidic degradative organelle that receives macromolecular cargo such as proteins, polysaccharides, and lipids from endocytosis, phagocytosis, and autophagy. The catabolic products of these macromolecules re-enter the cytoplasm to be used in biosynthesis reactions in the cell. The myriad forms of lysosomal storage diseases highlight the crucial role that catabolism and export of lysosomal macromolecules play in cell and organ functions (1). While lysosomal transporters for amino acids, monosaccharides, and ions have been characterized, less is known about the identity of lipid transporters (2–4), with the exception of Niemann-Pick C1 protein and Niemann-Pick C2 protein that critically mediate cholesterol transport out of lysosomes (5, 6). While not as well studied as for cholesterol, a similar lysosomal salvage pathway is known for sphingolipids (7) that is important for the metabolism of sphingolipid-like drugs such as FTY720 (8). Remarkably, there is a lack of information on the fate of glycerophospholipids within lysosomes, the main components of cellular membranes. In 1969, Fowler et al (9) were the first to describe that the end products of phosphatidylcholine (PC) and phosphatidylethanolamine (PE) catabolism in lysosomes are lysophosphatidylcholine (LPC), lysophosphatidylethanolamine (LPE), and fatty acid, consistent with the existence of lysosomal phospholipase A_1 and A_2 activities, with PLA2G15 being the only biochemically characterized mammalian lysosomal phospholipase A_2 (PLA_2) to date (10–12). We reasoned that because LPC and LPE molecules are zwitterionic and do not readily diffuse across membranes, they require a transporter to egress out of lysosomes to be reacylated by membrane bound O-acyltransferases (MBOATs) and LPC acyltransferases (LPCATs) located in the endoplasmic reticulum (ER) to form PC and PE (13) (Fig. 1*A*). Mfsd2a, a sodium-dependent LPC transporter and a member of the major facilitator superfamily (MFS), establishes the precedence for the requirement of a transporter for LPC and LPE across the plasma membrane of many cell types (14, 15). The other known lysolipid transporters that are part of the MFS family are Mfsd2b and Spns2, which both transport sphingosine-1-phosphate (S1P) at the plasma membrane (16, 17). These findings raise the possibility that an MFS transporter exists to mediate lysosomal efflux of LPC and LPE for phospholipid salvage.

Significance

Lysosomes mediate the hydrolysis of macromolecules for which the breakdown products must be transported out, failure of which could result in lysosomal storage diseases. While lysosomal transporters for amino acids, monosaccharides, and ions have been characterized, less is known about the identity of lipid transporters, particularly whether lysosomes export lysophospholipids that are breakdown products of phosphatidylcholine and phosphatidylethanolamine, the most abundant membrane phospholipids. This study combined a cell-based screen with biochemical, cell, and in vivo models to identify SPNS1, a previously orphaned transporter, as the transporter that mediates the rate-limiting lysosomal efflux of lysophospholipids for their recycling into cellular phospholipid pools. The deorphanization of SPNS1 sets a foundation for studying the role of lysolipid transport and recycling in physiology and disease.

Competing interest statement: D.L.S. is a scientific founder and advisor of Travecta Therapeutics, which has developed a drug delivery platform that uses MFSD2A transport. The remaining authors declare no competing interests.

This article is a PNAS Direct Submission.

[1]M.H. and A.C.Y.K. contributed equally to this work.

[2]To whom correspondence may be addressed. Email: david.silver@duke-nus.edu.sg or bchfdtt@nus.edu.sg.

This article contains supporting information online at http://www.pnas.org/lookup/suppl/doi:10.1073/pnas.2210353119/-/DCSupplemental.

Published September 26, 2022.

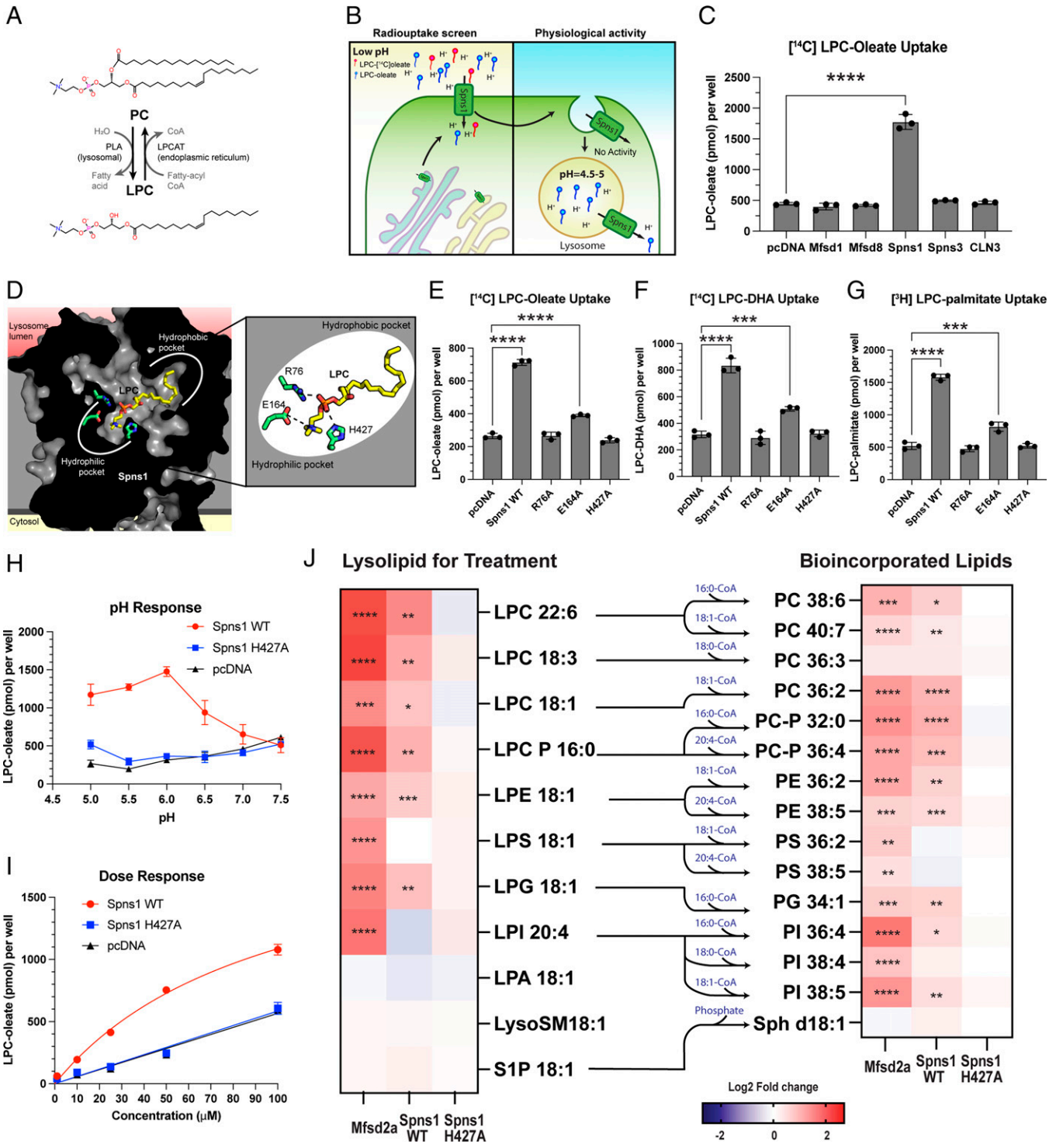

Fig. 1. Cell-based transport assay shows that Spns1 is an LPC transporter. (*A*) Illustration of Lands' cycle. CoA, coenzyme A. (*B*) Illustration of physiological activity of Spns1 and experimental setup for transport screen. (*C*) Uptake of 20 μM [^{14}C]-LPC-oleate in pH 5 buffer by MFS proteins. (*D*) Docking of LPC-oleate into binding pocket of a homology model of Spns1. (*E–G*) Transport activities of Spns1 mutants. DHA, docosahexaenoic acid. (*H*) pH dependency of uptake of 20 μM [^{14}C]-LPC-oleate by WT Spns1, H427A mutant, and empty plasmid. (*I*) Dose-response curve of [^{14}C]-LPC-oleate uptake by WT Spns1 and H427A mutant and pcDNA. (*J*) Ligand specificity of Spns1 determined by mass uptake of transported lysolipids in pH 6 buffer and the amount of their corresponding bio-incorporated lipids measured by targeted lipidomics. Heatmaps show $\log_2$-fold change calculated against levels in pcDNA-transfected cells. Cells with asterisks indicate a significant change relative to pcDNA. (*A–I*) n = three replicates; data are expressed as mean +/− SD. *P < 0.05; **P < 0.01; ***P < 0.001; ****P < 0.0001; one-way ANOVA with Dunnett's test.

Results

Spns1 is an LPC/LPE Transporter. We therefore screened a panel of ubiquitously expressed orphan MFS proteins that are known to be localized to the lysosome and that have amphipathic binding pockets suitable for lysolipid transport (15, 18–21). Since many lysosomal transmembrane proteins traffic through the plasma membrane (PM) before entering the endocytic pathway (22), an exporter protein at the lysosome membrane can function as an importer at the PM if it is exposed to substrate and a proton gradient (Fig. 1*B*). We took advantage of this cellular phenomenon to devise a cell surface uptake assay to screen

for LPC transporters. We overexpressed orphan candidate transporters in HeLa cells and verified that they accumulated at the PM by using cell surface biotin cross-linking (*SI Appendix*, Fig. S1*A*). Placing cells in buffer at pH 5 to mimic the acidic luminal environment of lysosomes and measuring the uptake of [^{14}C]-LPC-oleate into cells, we found that Spns1 was the only MFS in the panel that showed a significant increase in [^{14}C]-LPC-oleate uptake relative to control (Fig. 1*C*). Spns1 did not mediate the uptake of [^{3}H]-sphingosine, a lysolipid-like molecule structurally different from LPC (*SI Appendix*, Fig. S1*B*). Alanine mutagenesis of phylogenetically conserved residues arginine 76 (R76), glutamate 164 (E164), and histidine 427 (H427), which are predicted to form salt bridges with the choline and phosphate moieties of LPC (Fig. 1*D*), abolished or significantly reduced the uptake of [^{14}C]-LPC-oleate (Fig. 1*E*). We verified that all mutants were expressed at the PM and that H427A mutant was expressed at levels similar to those of wild-type (WT) Spns1 (*SI Appendix*, Fig. S1 *C* and *D*). Henceforth, we chose H427A as a negative control. Spns1 is also able to transport [^{14}C]-LPC-DHA and [^{3}H]-LPC-palmitate, indicating a general activity toward LPCs with saturated, monounsaturated, and polyunsaturated fatty acids (Fig. 1 *F* and *G*). We further demonstrated that WT Spns1, but not the H427A mutant, can mediate mass uptake of LPC-DHA and increase the cellular mass of PC-DHA as revealed by thin-layer chromatography (*SI Appendix*, Fig. S1*E*). The increase in PC-DHA indicated that LPC-DHA was bio-incorporated into PC, further supporting the conclusion that Spns1 mediates LPC transport and not simply LPC binding to Spns1 at the PM. The uptake of [^{14}C]-LPC-oleate by Spns1 was concentration dependent and saturable, with a pH optimum between pH 5.0 and 6.0 (Fig. 1 *H* and *I*), indicating that Spns1 is a proton-coupled LPC transporter.

To define the ligand specificity of Spns1 transport, we used our cell surface transport assay coupled with lipidomics to quantify uptake of lysolipids and their bio-incorporation into re-esterified phospholipid species, using Mfsd2a as a positive control (Fig. 1*J* and *SI Appendix*, Fig. S2). Spns1 transported lysophospholipids with zwitterionic headgroups such as LPC and LPE. That Spns1 transported lyso-plasmalogen, an LPC with a fatty alcohol, indicated that the carbonyl group of the fatty acyl chain is not an essential feature of an Spns1 ligand. With the exception of lysophosphatidylglycerol (LPG), we could not detect transport of the anionic lysophospholipids lysophosphatidylserine (LPS), lysophosphatidylinositol (LPI), and lysophosphatidic acid (LPA). Lyso-sphingomyelin (lyso-SM) and S1P were not transported by Spns1, indicating it has a distinct substrate selectivity primarily for LPCs and LPEs, unlike its paralog Spns2 which transports S1P (23). The observed higher activity of Mfsd2a over Spns1 in this assay for LPC and LPE is likely explained by the higher cell surface expression of Mfsd2a, which evolved to function at the PM, while Spns1 transiently traffics through the PM. Overall, our results highlight an exquisite substrate selectivity of Spns1 for LPC, LPE, and LPG.

Spns1 Deficiency in Mammalian Cells Results in Lysosomal Accumulation of LPC and LPE. To investigate the function of endogenous Spns1 in the lysosome, we generated Spns1 knockout (KO) HEK293T cells using CRISPR/Cas9. Importantly, Spns1 KO cells displayed increased levels of total LPC and LPE, as determined by mass spectrometry (*SI Appendix*, Fig. S3 *B* and *C*), providing the first biochemical evidence that Spns1 deficiency leads to cellular accumulation of LPC and LPE. On the basis of Spns1 KO efficiency and the extent of LPC and LPE accumulation, we chose to use KO1 (gRNA1) for further investigation and henceforth designated it as Spns1 KO (*SI Appendix*, Fig. S3 *A–C*). Spns1 KO cells showed enlarged lysosomes detected as Lysotracker-positive compartments (Fig. 2*A*) and increased basal LC3b levels (Fig. 2*B*), indicating that Spns1 deficiency leads to defects in lysosome size and autophagy, phenotypes previously seen in Spns1-deficient cells (24–26).

We next investigated the effects of Spns1 deficiency on the lysosome lipidome by using superparamagnetic iron oxide nanoparticles (SPIONs) to obtain lysosome-enriched fraction (*SI Appendix*, Fig. S3 *D–F*). As a first approach to determine whether Spns1 deficiency would lead to elevation of lysosomal LPCs, we metabolically labeled cellular phosphatidylcholine, SM, and LPC pools with [^{14}C]-choline and isolated lysosomes. Remarkably, [^{14}C]-labeled LPC was increased approximately five-fold in lysosome-enriched fraction from Spns1 KO cells relative to control cells (Fig. 2 *C* and *D*). In an independent label-free lipidomic approach, we observed a 1.48- to ∼4.91-fold increase of all quantified LPCs and LPEs in the lysosome-enriched fraction of Spns1 KO cells relative to control cells, which was rescued by re-expressing Spns1, which is consistent with these phenotypes being Spns1 dependent (Fig. 2 *E* and *F*). We also noted a large increase in the level of lysosomal sphingosine (Fig. 2*E*). Since sphingosine is not transported by Spns1 (*SI Appendix*, Fig. S1*B*), this increase is interpreted as a secondary effect of Spns1 deficiency. A similar accumulation of LPCs and LPEs was found in whole cells (Fig. 2*F*). Taken together, these data indicate that endogenous Spns1 mediates the transport of LPCs and LPEs out of lysosomes and is critical for maintaining cellular homeostasis of LPCs and LPEs.

Spns1 Mediates a Lysosomal Salvage Pathway for Phospholipids. We reasoned that since Spns1 is required for lysosomal efflux of LPC and LPE, that loss of Spns1 should lead to less LPC and LPE available for re-acylation by LPCATs, the rate-limiting enzymes of the Lands' cycle in the ER. To test this hypothesis, we pulse-labeled control and Spns1 KO cells with [^{14}C]-oleic acid, which is used in re-acylation of LPCs into PC (*SI Appendix*, Fig. S4*A*). Spns1 KO cells exhibited 25% less [^{14}C]-oleic acid incorporated into PC relative to control cells during a 30-min labeling time (*SI Appendix*, Fig. S4*B*). Chemical inhibition of autophagosome formation and fusion or inhibition of lysosomal phospholipase activity that produces LPC normalized the level of [^{14}C]-oleic acid incorporation into PC between Spns1 KO and control cells (*SI Appendix*, Fig. S4 *B–D*). Taken together, these findings indicate a Spns1-dependent contribution to lysosomal LPC efflux used for re-acylation into PC.

We next sought to directly measure the in vivo flux of LPCs out of lysosomes and their subsequent re-acylation by following the fate of stable isotope-labeled PC (d9-PC 36:2; structure shown in Fig. 3*A*) delivered to lysosomes. If Spns1 indeed transports LPC out of lysosomes, we predicted that lysosome-derived d9-LPC species will be re-acylated by LPCATs at the ER to produce d9-containing PC species with various types of fatty acyl chains in addition to 18:1 (Fig. 3*A*). To selectively deliver d9-PC 36:2 to lysosomes, we took advantage of the specific binding of apolipoprotein E (apoE) to low-density lipoprotein receptor (LDLR) and generated d9-PC 36:2 nanodiscs containing apoE to drive LDLR-dependent endocytosis and subsequent delivery to lysosomes (27). Enrichment of d9-PC 36:2 over nondeuterated PC 36:2 in the lysosome-enriched fraction was significantly higher when cells were loaded for 3 h with apoE-complexed d9-PC 36:2 nanodiscs compared with cells loaded with d9-PC 36:2 nanodiscs without apoE (Fig. 3*B*), demonstrating apoE-dependent targeting

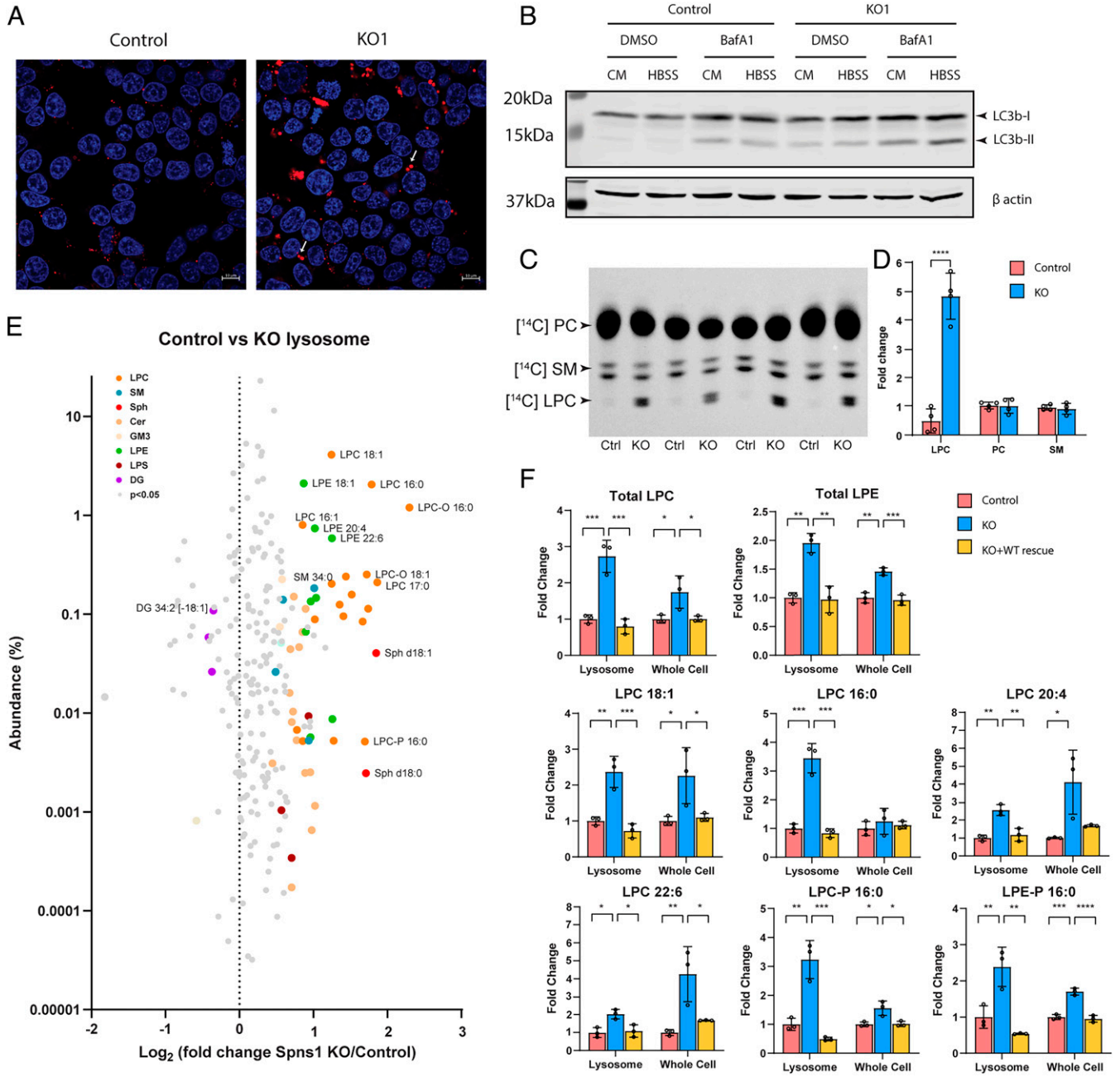

Fig. 2. Spns1 KO cells accumulate LPC in lysosomes. (*A*) Live-cell LysoTracker staining of Spns1 KO HEK293T cells or nontargeting gRNA (control). Scale bar, 10 μM. Arrows indicate enlarged lysosomes in KO cells. Blue, Hoechst stain; red, Lysotracker stain. Representative images of four independent experiments. (*B*) Immunoblot analysis of LC3b-I and LC3b-II levels on control and KO cell lysates from cells grown in complete medium (CM) or grown for 1 h in Hank's balanced salt solution (HBSS) with or without 5-h pretreatment with 100 nM bafilomycin A1 (BafA1). DMSO, dimethyl sulfoxide. Western blot is representative of four independent experiments. (*C*) Lysosomes isolated from [^{14}C]-choline–labeled Spns1 KO cells showed accumulation of [^{14}C]-LPC (representative of four independent replicates). (*D*) Quantification of phosphor images in panel (*C*). (*E*) Lipidomic analysis of lysosome-enriched fraction obtained using the SPION method from control and Spns1 KO cells. Mean lipid abundance was calculated as mole percentage of each lipid species per gram of protein, with colored dots indicating significantly different lipid species in KO relative to control (n = three independent replicates). Cer, ceramide; DG, diacylglycerol; GM3, ganglioside; Sph, sphingosine. (*F*) Fold change of selected LPC and LPE species in whole cells or lysosome-enriched fraction from control, Spns1 KO, and Spns1 KO cells stably transduced with Spns1 WT rescue plasmid; n = three independent replicates for (*E*) and (*F*). Data are represented as mean +/− SD. *P < 0.05; **P < 0.01; ***P < 0.001; ****P < 0.0001; (*D* and *E*) two-sided Student t test; (*F*) one-way ANOVA with Tukey's test.

of lysosomes. Importantly, and in agreement with Spns1 KO cells accumulating LPC (Fig. 2 *E* and *F*), d9-LPC 18:1 accumulated to a greater extent in the lysosome-enriched fraction of Spns1 KO cells relative to control cells treated with d9-PC 36:2 apoE-complexed nanodiscs (Fig. 3*C*). These findings further support the hypothesis that LPC is the breakdown product of PC in lysosomes (9) and that Spns1 regulates the levels of lysosomal LPC.

We next measured the amount and diversity of d9-containing phospholipid species after loading cells with d9-PC 36:2 apoE nanodiscs. The total amount of d9-choline–containing lipid species was similar between Spns1 KO and control cells at all time points tested (Fig. 3*D*), indicating that there is no defect in the LDLR-dependent endocytosis pathway in Spns1 KO cells. Critically, Spns1 KO cells accumulated d9-LPC 18:1 at all time points relative to control cells (Fig. 3*E*). As early as the first hour

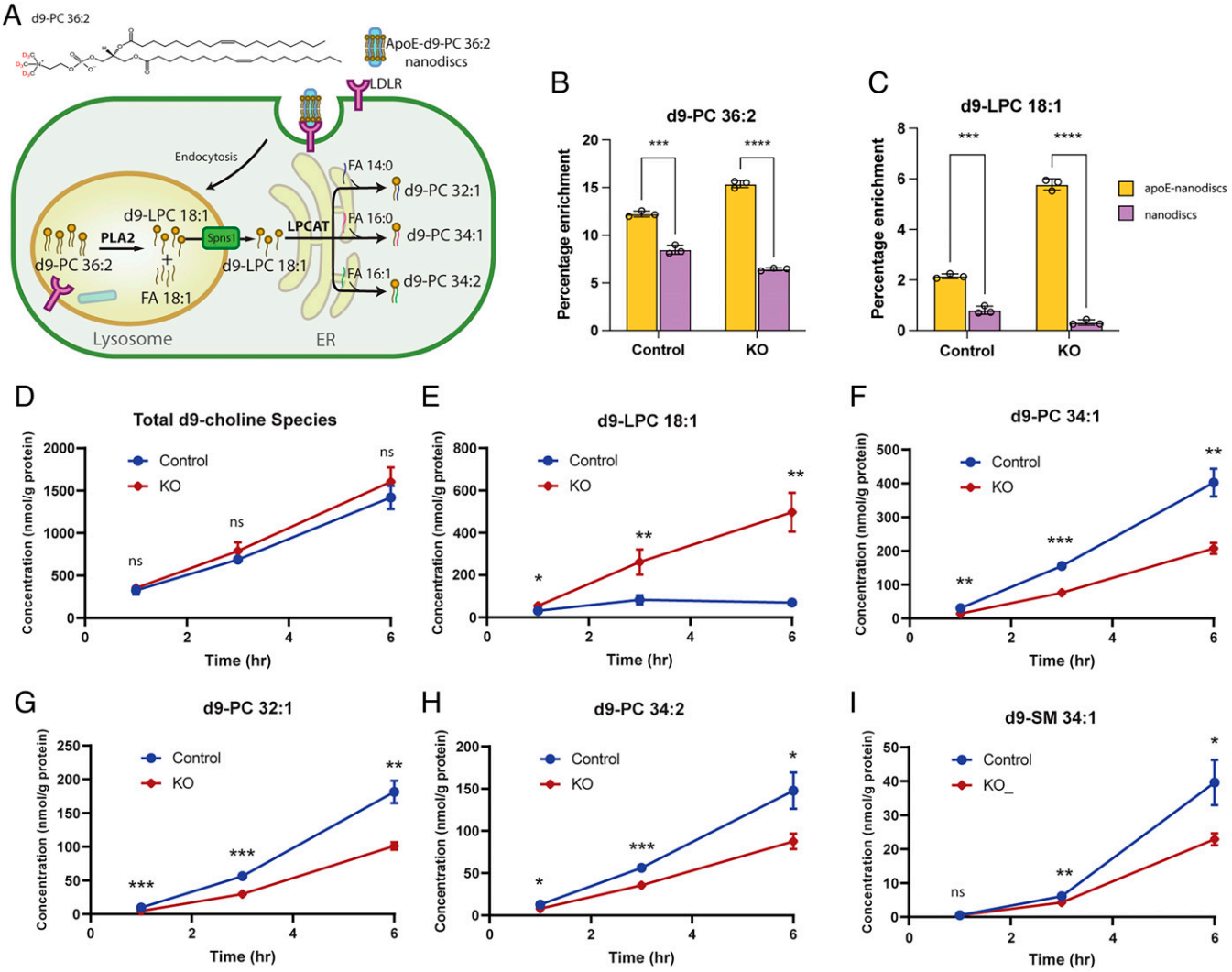

Fig. 3. Spns1 mediates lysosomal efflux of LPC that reenters phospholipid pools. (*A*) Illustration of experiment design using nanodiscs of apoE-complexed deuterated-PC 36:2. MS measurement of d9-PC 36:2 (*B*) and d9-LPC18:1 (*C*) in lysosome-enriched fraction obtained using SPION method after 3 h of loading with nanodiscs of apoE-complexed d9-PC 36:2 and d9-PC 36:2 alone. MS measurement of total cellular d9-choline–containing lipids (*D*), d9-LPC 18:1 (*E*), d9-PC 34:1 (*F*), d9-PC 32:1 (*G*), d9-PC 34:2 (*H*), and d9-SM 34:1 (*I*) after 1 h, 3 h, and 6 h loading with nanodiscs of apoE complexed d9-PC 36:2 (n = three independent replicates). Data are represented as mean +/− SD. ns, not significant; FA, fatty acid. *$P < 0.05$; **$P < 0.01$; ***$P < 0.001$; ****$P < 0.0001$; two-sided unpaired Student *t* test.

of d9-PC 36:2 loading, control cells synthesized twofold more d9-PC 32:1, d9-PC 34:1, and d9-PC 34:2 relative to Spns1 KO cells (Fig. 3 *F*–*H*). These PC species are generated by re-acylation of lysosome-derived d9-LPC 18:1 with 14:0, 16:0, and 16:1 fatty acyl-coenzyme A (acyl-CoA) donors, respectively. The reduction in d9-PC formation in Spns1 KO cells persisted up to the 6-h time point. Furthermore, Spns1 KO cells produced less d9-containing sphingomyelin (SM) (d9-SM), particularly at later time points, which is consistent with the formation of this lipid requiring an additional step of d9-choline transfer from PC onto ceramide to form SM by SM synthase (Fig. 3*I*). While d9-PC species in Spns1 KO cells were reduced compared with those in control cells, we still observed low but significant production of d9-PC species in Spns1 KO cells, which can likely be attributed to lysosome-independent uptake of apoE nanodiscs as surmised by the cellular uptake of nanodiscs devoid of apoE (Fig. 3*B*). Taken together, data from our flux analysis support the conclusion that LPCs are transported out of lysosomes by Spns1 and re-acylated into PC pools, thus constituting a lysosomal salvage pathway for LPC, and by extension LPE, another abundant lysophospholipid produced in the lysosome and transported by Spns1 (Fig. 1*J*).

Spns1 deficiency in zebrafish embryos and mouse liver results in accumulation of LPC and LPE with pathological consequences. To test the role of Spns1 in mediating lysosomal LPC and LPE efflux in a multicellular organism, we first used zebrafish as a model system. Spns1 knockdown (KD) in zebrafish embryos has been reported to cause yolk sac opacity and lethality at early larval stages (28), but a molecular explanation for this phenotype was unknown. Lipidomic analysis on Spns1-deficient whole embryos revealed significant accumulation of LPC and LPE species relative to control embryos (*SI Appendix*, Fig. S5), consistent with the molecular function of Spns1 as an LPC and LPE transporter.

Because there is no information on Spns1 function in mammals, we performed short hairpin RNA (shRNA)-mediated KD of Spns1 in livers of adult mice using adeno-associated virus 8 (AAV8). Liver is rich in lysosome activity for lipoprotein processing, autophagy, and energy metabolism and can thus serve as a model for studying the function of Spns1 at the organ level. Spns1 KD efficiency was verified by qRT-PCR and western blot of a lysosome-enriched fraction (*SI Appendix*, Fig. S6 *A*–*C*). The level of serum alanine aminotransferase (ALT) was

significantly elevated in Spns1 KD mice, indicating liver damage (Fig. 4*A*). Serum cholesterol, but not triglycerides, was also elevated in Spns1 KD mice (Fig. 4*B*). While there were no noticeable pathological changes upon histological examination of liver sections (Fig. 4*C*), immunofluorescent staining with lysosomal markers LAMP1 and cathepsin B revealed a remarkable increase in lysosome clusters at the perinuclear region of hepatocytes from Spns1 KD mice relative to control mice (Fig. 4*D*). Consistent with these findings, density gradient fractionation of Spns1 KD liver homogenate revealed enrichment of lysosomes in low-density fractions (fractions 1 and 2), while control showed enrichment of lysosomal markers in higher-density fractions (i.e., fraction 6)

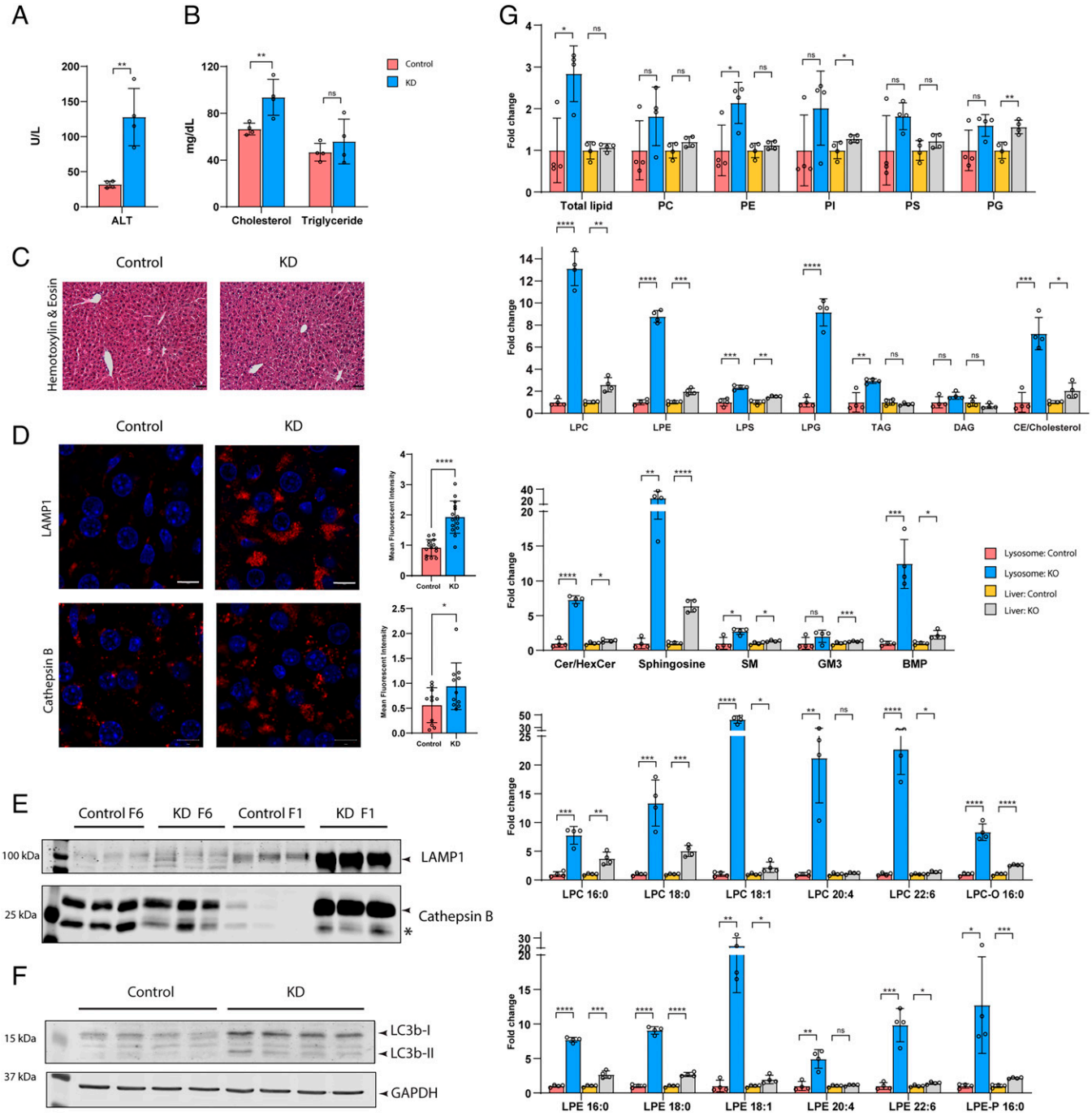

Fig. 4. Spns1 KD in liver elevates lysosomal LPCs and LPEs and results in abnormal lysosomes. Serum level of ALT (*A*) and total cholesterol and triglyceride (*B*) in mice at 4 wk after being injected with shRNA targeting Spns1 (KD) or nontargeting shRNA (control). (*C*) Hematoxylin and eosin stain of liver tissue sections. Scale bar, 50 μm. (*D*). Immunofluorescent staining of LAMP1 (red) and cathepsin B (red) in liver sections. Blue, Hoechst stain. Mean fluorescent intensity of LAMP1 and cathepsin B was quantified from cells in experiments with three mice per group (scale bar, 10 μm). (*E*) Immunoblotting of LAMP1 and cathepsin B in lysosome-enriched fractions (F1 and F6) obtained from OptiPrep density gradient fractionation of livers from Spns1 KD and control mice. Upper cathepsin B band (27 kDa, indicated by an arrow head) is the glycosylated form, and the lower band (24 kDa, indicated by an asterisk) is the deglycosylated form. (*F*) Immunoblotting of LC3b-I and LC3b-II from liver lysates. (*G*) Lipidomics analysis of lysosome-enriched fractions (fractions 1, 2, and 6 combined) relative to whole tissue from control and KD mice. BMP, bismonoacylglycerophosphate; CE, cholesterol ester; Cer/HexCer, ceramide/hexosylceramide; DAG, diacylglycerol; PG, phosphatidylglycerol; PI, phosphatidylinositol; PS, phosphatidylserine; TAG, triglyceride. (*A*–*C*, *E*–*G*) n = four mice per group. (*A*, *B*, *D*, *G*) Data are represented as mean +/− SD. **P* < 0.05; ***P* < 0.01; ****P* < 0.001; *****P* < 0.0001; two-sided unpaired Student *t* test.

(*SI Appendix*, Fig. S6 *D–F*). Furthermore, these low-density lysosomes in Spns1 KD livers showed an increased ratio of glycosylated:de-glycosylated form of cathepsin B (Fig. 4*E* and *SI Appendix*, Fig. S6*F*), indicative of lysosome alkalinization (29). In addition, Spns1 KD liver showed an increased level of LC3b-I and LC3b-II (Fig. 4*F*), suggesting a block in autolysosome formation.

We next tested whether Spns1 KD in liver resulted in elevated lysosomal LPCs and LPEs. Lipidomics analysis of lysosome-enriched fractions (sum of F1, F2, and F6) revealed an 8-fold to 13-fold accumulation of total and individual species of LPCs, LPEs, and LPGs in Spns1 KD lysosome-enriched fractions (Fig. 4*G* and *SI Appendix*, Fig. S6*G*), consistent with the function of Spns1 as a lysosomal lysophospholipid exporter. Such accumulation was significant enough to be observed in whole-cell lysates without subcellular fractionation, especially for LPCs and LPEs containing saturated fatty acyl chains, such as LPC 16:0 and LPC 18:0 (Fig. 4*G* and *SI Appendix*, Fig. S6*G*). We also observed enrichment of other lipid classes in Spns1 KD lysosomes. In fact, the total lipid content normalized to protein content was threefold higher in Spns1 KD lysosomes, consistent with an increase in lysosome number as revealed by an increase in LAMP1 immunofluorescence (Fig. 4 *D* and *G*). Bismonoacylglycerophosphate (BMP), a characteristic anionic glycerophospholipid found exclusively in intraluminal membranes of late endosomes and lysosomes, was 12-fold higher in Spns1 KD lysosomes compared with control lysosomes, suggesting an expansion of intralysosomal membranes (Fig. 4*G*). Notably, SM and ganglioside metabolites, including hexosylceramide, ceramide, and sphingosine, as well as cholesterol and cholesteryl esters, were highly enriched in Spns1 KD lysosomes (Fig. 4*G* and *SI Appendix*, Fig. S6*G*). Such changes in lipid profile resemble other lysosomal lipid storage diseases such as Niemann-Pick C2 disease and Gaucher disease (6, 30, 31). The observed lipid enrichment cannot be fully attributed to the increase in size and number of lysosomes because structural phospholipids, including PC and PE, showed only a modest twofold to threefold accumulation relative to controls, similar to the fold change observed for total lipid content (Fig. 4*G*). It is likely that Spns1 deficiency leads to lysosomal dysfunction such as luminal alkalization, which is expected to negatively impact the functions of enzymes involved in sphingolipid and cholesteryl ester metabolism.

To investigate the longer-term effects of Spns1 deficiency, we examined mice at 8 wk after injection of AAV8. The enlargement of lysosomes, elevation of LC3b-II, and tissue level accumulation of LPCs and LPEs persisted (*SI Appendix*, Fig. S7 *A–F*). Notably, there was lobular inflammation in liver shown by increased number and clustering of galectin 3–positive immune cells, and elevated serum ALT (*SI Appendix*, Fig. S7*G* and Fig. 7*B*). Gene enrichment analysis derived from RNA sequencing from these livers was in agreement with increased inflammation (*SI Appendix*, Fig. S7*H*).

Discussion

This study identifies Spns1 as the transporter that mediates the rate-limiting lysosomal efflux of LPC and LPE, which uncovered the existence of a lysosomal salvage pathway for LPC and LPE derived from catabolism of PC and PE, the two most abundant phospholipids of eukaryotic membranes. We observed that Spns1 deficiency had pleiotropic effects in cells and mouse liver, including inflammation, secondary accumulation of multiple lipid species in lysosomes, and impaired autophagy, similar to other lysosomal lipid storage diseases such as Niemann-Pick disease type C (NPC) , GM1 gangliosidosis, and Gaucher disease (32). The majority of lysosomal lipid storage diseases are due to mutations in luminal enzymes that break down lysosomal lipids, with NPC1 being the only known lipid transporter directly linked to a lysosomal lipid storage disease. Spns1 deficiency could represent another example of a lysosomal storage disease that results from the loss of lipid transporter activity, but whether such a disease resulting from mutations in *Spns1* exists in humans remains to be determined. Previous reports demonstrated that Spns1 deficiency leads to defective autophagosome-lysosome fusion in zebrafish (25) and defective autophagic lysosome reformation after starvation in a cultured cell line (24). Moreover, deficiency of *Spin*, the drosophila ortholog of Spns1, resulted in defects in endosome-to-lysosome trafficking with synaptic dysfunction (33). However, because the ligand for Spns1 was not known and hence its function was unknown, the molecular basis for explaining these phenotypes remained unclear. An asymmetrical distribution of lysolipids, including cone-shaped LPC, can lead to positive membrane curvature, which is important for membrane fusion and is proposed to be important for autophagosome-lysosome fusion (34). Importantly, model membrane systems have shown that high levels of LPC can inhibit membrane fusion (35, 36). It is plausible that the defects in autophagosome-lysosome fusion and lysosome reformation in Spns1-deficient cells could in part be a result of the effects of markedly elevated lysosomal LPC and LPE on membrane dynamics. Consistent with negative effects of elevated LPC on lysosomal membrane dynamics, CRISPR/Cas9 genome-wide screens identified that Spns1 deficiency reduced host cell infection by a common cold coronavirus and Ebola virus that require fusion with the lysosome membrane during the infection process (37, 38).

This discovery that Spns1 is an LPC/LPE transporter in contrast to the S1P transporter Spns2 remarkably mirrors that of Mfsd2a (LPC/LPE transporter) and Mfsd2b (S1P transporter) (17, 23). It is notable from an evolutionary perspective that despite being functionally similar, the LPC/LPE transporters Spns1 and Mfsd2a (also Spns2 and Mfsd2b) lack sequence similarity beyond being in the same superfamily, which suggests that parallel evolutionary processes are at play for selecting the same substrate specificity, albeit for transporters expressed at different subcellular locations. A recently solved cryo-electron microscopy structure of Mfsd2a bound to LPC suggested that it functions as a lysolipid flippase (15). It is possible that Spns1 may function by an analogous mechanism, although biochemical evidence for such a mechanism remains to be determined for both Mfsd2a and Spns1. Interestingly, LPS is transported by Mfsd2a but not by Spns1. This substrate specificity correlates with the finding that LPS might not be generated from PS in lysosomes (9), suggestive of a lack of selective pressure for binding LPS. We also note from our mass uptake lipidomics data that both Spns1 and Mfsd2a seem to transport LPG, a ligand that we had not tested in previous studies of Mfsd2a. This suggests hitherto undetermined aspects in the substrate specificity of these lipid transporters. Whether LPG is a physiological ligand for Spns1 and what role LPG recycling may play in cellular function require further study. Given the centrality of lysosomes in cellular homeostasis, the deorphanization of Spns1 provides new opportunities for studying the role of lysolipid transport and recycling in physiology and disease.

Materials and Methods

Cell Culture. HEK293T and HeLa cells were obtained from the American Type Culture Collection and grown in Dulbecco's modified Eagle medium (DMEM; HyClone) supplemented with 10% heat inactivated fetal bovine serum (FBS)

(Gibco) plus penicillin and streptomycin (Gibco) at 37 °C with 5% CO_2. FBS was delipidated according to Hannah et al (39) and used at 5% delipidated FBS in DMEM in experiments that used delipidated media.

Generation of cDNA Constructs. Codon optimized complementary DNAs (cDNAs) for human SPNS1, SPNS3, MFSD1, MFSD2A, MFSD8, MFSD12, and CLN3 were synthesized by GenScript and cloned into a pcDNA3.1 plasmid with or without a C-terminal Myc-6His Tag. Mouse Spns1 cDNA was isolated by PCR from a cDNA library of an RAW264.7 cell and cloned into pcDNA3.1 plasmid. SPNS1 mutants were generated by the QuikChange site-directed mutagenesis method (Agilent) (40).

Cell Surface Transport Assay. HeLa cells transfected with plasmid encoding indicated constructs for 24 h were washed once with reaction buffer before incubating with the indicated concentration of radiolabeled ligands in 0.5 mL reaction buffer for 30 min at 37 °C with 5% CO_2. Cells were washed twice with 0.5% (wt/vol) fatty acid–free bovine serum albumin (BSA) (Sigma) in reaction buffer and then extracted twice with 1% Triton X-100 in tris(hydroxymethyl)aminomethane (Tris)-buffered saline. Extracts were transferred to 4 mL of EcoLite(+) scintillation fluid (Avantor) for scintillation counting using a Tri-Carb 2910 TR Liquid Scintillation Analyzer (PerkinElmer). List of and preparation of radiolabeled lipids are found in *SI Appendix, Supplementary Methods*. The following are reaction buffer compositions for each specified pH: pH 5.0: 25 mM sodium acetate, 150 mM NaCl, 5 mM glucose, 1 mM $MgCl_2$; pH 5.5: 25 mM sodium citrate, 150 mM NaCl, 5 mM glucose, 1 mM $MgCl_2$; pH 6.0 and pH 6.5: 25 mM sodium 2-(N-morpholino)ethanesulfonate (MES), 150 mM NaCl, 5 mM glucose, 1 mM $MgCl_2$; pH 7.0 and pH 7.5: 25 mM sodium *N*-2-hydroxyethylpiperazine-*N*′-2-ethanesulfonic acid (HEPES), 150 mM NaCl, 5 mM glucose, 1 mM $MgCl_2$. For the bulk transport assay, cells were incubated with 50 μM of each specified lipid in pH 6.0 buffer for 1 h. Cells were then washed twice with 0.5% (wt/vol) fatty acid–free BSA in phosphate-buffered saline (PBS) to remove excess ligand and washed once again with PBS to remove BSA. After lipid extraction, the remaining cell skeleton on plates after hexane:isopropanol extraction was dissolved in 0.1% sodium dodecyl sulfate in 0.1 M NaOH for 4 h to determine protein concentration with the Pierce BCA Protein Assay Kit. Radiolabeled ligands and lipids used in the experiments are listed in *SI Appendix, Supplementary Methods*.

Homology Modeling of Human Spns1 and Docking of LPC-oleate. Homology model of the luminal-facing conformation of human Spns1 was constructed by I-TASSER (41) using the outward-facing crystal structure of human MFSD10 (Protein Data Bank ID: 6S4M) as a preferred template. Model of the cytosol-facing conformation of human Spns1 was obtained from the AlphaFold database (42). In silico docking of LPC-oleate to Spns1 was performed as described in *SI Appendix, Supplementary Methods*.

Generation of SPNS1 CRISPR/Cas9 KO Cell Line and Rescue Cell Line. KO cell lines were generated by infecting HEK293T cells with lentivirus carrying single guide RNA (sgRNA) directed against exon 1 of SPNS1 in lentiCRISPRv2 plasmid (Addgene, 52961). Guide RNA (gRNA) sequences are as follows: gRNA1: 5′-CTACATGGACCGCTTCACCG-3′; gRNA2: 5′- CCGTTCGGCTCTCATAGTGG-3′; gRNA3: 5′-CGTGGACCCTGGCAACCCCG-3′; gRNA4: 5′-CCGCCACTATGAGAGCCGAA-3′; gRNA5: 5′-CGGGGTTGCCAGGGTCCACG-3′; gRNA6: 5′-CTCGGACTTCGGGTTCCCCG-3′. The scrambled gRNA used for control cells was 5′-GTGTAGTTCGACCATTCGTG-3′. For SPNS1 WT rescued plasmid, a codon-optimized SPNS1 sequence under a minipTK promoter (from pTK-HSV-BP2; ATCC), followed by internal ribosome entry site (IRES; from pIRES2-EGFP) was cloned by the Gibson Assembly (43) method into a lentiCas9-Blast plasmid (Addgene, 52962) which has the cytomegalovirus (CMV) promoter and Cas9 sequence excised. Procedures for viral particle production, cell infection, and selection are described in *SI Appendix, Supplementary Methods*.

LysoTracker Staining. Cells were stained with 50 nM LysoTracker Red (Thermo Fisher Scientific) in medium for 30 min. Hoechst 33342 (1:1,000) (Thermo Fisher Scientific) was added to the medium in the final 10 min. Cells were imaged live using an LSM710 confocal microscope (Carl Zeiss).

Isolation of Lysosomes From Cultured Cells and Mouse Liver. Isolation of lysosomes from cultured cells was carried out according to Thelen et al (44). Details are provided in *SI Appendix*. To prepare lysosome enriched fraction from mouse liver, freshly harvested mouse livers were minced in 10 mL/g of liver weight of homogenization buffer (HB; 0.25 M sucrose, 10 mM HEPES, 1 mM ethylenediaminetetraacetic acid [EDTA], cOmplete Protease Inhibitor), and homogenized with six strokes in a glass homogenizer. The homogenate was centrifuged at 1,000 *g* for 10 min. The resulting pellet was homogenized again in 5 mL/g of liver weight of HB and centrifuged again to generate postnuclear supernatant (PNS). These two PNSs were combined and centrifuged for 10 min at 3,000 *g* to remove heavy mitochondria. The resulting supernatant was centrifuged at 20,000 *g* for 20 min to pellet a light mitochondria fraction (LMF). The LMF was resuspended and loaded into a discontinuous OptiPrep density gradient (with density steps of 8%, 12%, 16%, 19%, 22.5%, 27%) and ultracentrifuged at 150,000 *g* for 4 h in an SW41 rotor (Beckman Coulter). The gradient was collected from the top of the gradient to the bottom. β-N-acetylglucosaminidase activity of PNS, LMF, and each fraction was determined by using a β-N-acetylglucosaminidase assay kit (Sigma, CS0780). Protein concentration was determined by Pierce BCA Protein Assay Kit. For *SI Appendix*, Fig. S6*F*, 2.5% (by volume) of each fraction was loaded for western blot analysis. Equal amounts of protein were loaded for Fig. 4*E* and *SI Appendix*, Figs. S3*D* and S6*C*.

[^{14}C]-Choline Labeling of Cells. For metabolic labeling of cells with [^{14}C]-choline, cells were grown in 10-cm dishes and were labeled with 4 mL of choline-deficient DMEM plus 10% FBS containing 0.2 μCi of [^{14}C]-choline (American Radiolabeled Chemicals, specific activity: 50 mCi/mmol) for 24 h before harvesting for lysosome isolation.

ApoE-d9 PC-36:2 Nanodisc Generation and Cell Treatment. A total of 1.079 mg of d9-PC 36:2 (L-1182d, Echelon Biosciences) was dried in a nitrogen stream and reconstituted in 18.53 μL of Tris-buffered saline (TBS) (10 mM Tris HCl [pH 7.4], 150 mM NaCl, 0.25 mM EDTA, 0.0005% NaN_3). A total of 42.2 μL of sodium cholate (30 mg/mL) was added to the lipid suspension and incubated at room temperature for 30 min with shaking; then 100 μL of 5 mg/mL apoE3 (900010, Sigma) was added to the mixture and incubated at room temperature with rotation mixing for 1 h for apoE incorporation with into lipid discs. Sodium cholate was removed by incubating with 0.2215 g of BioBeads SM2 (Bio-Rad) overnight. The stock concentration of apoE-d9 PC-36:2 nanodiscs was 0.5 mg/mL apoE plus 1 mg/mL d9-PC-36:2, and aliquots were snap frozen and stored at −80 °C until further use. Nanodiscs with d9-PC-36:2 only were constructed in the same way, except that 100 μL of TBS was used instead of apoE3.

For delivery of apoE-d9 PC-36:2 nanodiscs into cells, cells were grown in delipidated medium for 24 h to upregulate LDLR before incubating with apoE-d9-PC-36:2 nanodiscs. For time course analysis, cells grown in 12-well plates were incubated with 15 μg apoE-d9 PC-36:2 nanodiscs/mL of medium (based on apoE concentration in the discs and equivalent to 22.6 nmol of d9-PC-36:2). For equivalent experiments that required lysosome isolation, cells were grown in 6-cm dishes and incubated with 12.5 μg apoE-d9 PC-36:2 nanodiscs/mL of medium (based on apoE concentration and equivalent to 67.85 nmol of d9-PC 36:2) for 3 h before SPION-mediated lysosome isolation.

Animals. All mice were bred and maintained at the Duke-National University of Singapore animal facility. The experimental protocols were performed in concordance and approved by SingHealth Institutional Animal Care and Use Committee (IACUC protocol #2015/SHS/1416). All mice were housed in 12-h light:12-h dark cycles with humidity and temperature-controlled environment at 23 °C. The mice were fed ad libitum with standard normal chow diet consisting of 12% fat, 23% protein, and 65% carbohydrate based on caloric content and given free access to water.

For the AAV8-*SPNS1* shRNA KD experiment, AAV8-*SPNS1* shRNA (5′-GCAG TTCTTTAACATCGGAGA-3′ (Vector Biolabs) or AAV8-scrambled shRNA control (Vector Biolabs) were injected into 8-wk-old C57BL/6NTAC mice via a retro-orbital venous route at a concentration of 5×10^{11} genome copies per mouse.

Four weeks after injection of AAV, mice fasted overnight and were then euthanized. Before being euthanized, mice were anesthetized with 200 mg/kg ketamine and 20 mg/kg xylazine in PBS, followed by blood collection via cardiac puncture to generate serum. Mice were then perfused with PBS before the liver was collected for lysosome isolation, snap-frozen in liquid nitrogen, or fixed in buffered formaldehyde solution. Measurement of blood parameters, histology, immunofluorescence, and immunohistochemistry of mouse tissue was performed as described in *SI Appendix, Supplementary Methods*. RNA from mouse liver was extracted using TRIzol and Rneasy spin column (QIAGEN) and reverse transcribed using iScript RT Supermix (Bio-Rad). qPCR was performed

using SensiFAST SYBR Hi-ROX (Bioline Agrosciences) with the following primers: for mouse SPNS1, forward: 5′- ACCTCCTGAACTACATGGAC-3′, reverse: 5′- CCAT GTAACTGGAGATGAAC-3′; for mouse β actin, forward: 5′-GGCTGTATTCCCCTCCA TCG-3′, reverse: 5′-CCAGTTGGTAACAATGCCATGT-3′ (PrimerBank ID: 6671509a1).

LC-MS/MS Analysis and Data Analysis. Sample preparation for lipidomics is described in *SI Appendix, Supplementary Methods*. The liquid chromatography-tandem mass spectrometry (LC-MS/MS) analysis and data analysis were performed as previously reported (45). Targeted analysis was performed in dynamic multiple reaction monitoring MS-positive and -negative (only when measuring LPA species) ion mode. Labeled lipids (PC, LPC, and SM) were monitored by increasing the mass divided by charge number of the precursor and fragment ion (when containing the labeled portion of the precursor) by 9 Da as a result of incorporation of the labeled choline group. Internal standards were used to normalize the raw peak areas in the corresponding lipid class, and concentrations were further normalized to the protein concentration in the original sample. For SPION or liver tissue fractionation, concentrations were further normalized to sample volume.

Statistical Analysis. Statistical analysis was performed using Graphpad PRISM for two-sided unpaired Student *t* test, and one-way ANOVA with Dunnett's test or with Tukey's test as indicated in the figure legends. Additional information can be found in *SI Appendix, Supplementary Methods*.

Data Availability. All study data are included in the article and/or supporting information.

ACKNOWLEDGMENTS. We thank Caroline Wee Lei, Institute of Molecular and Cellular Biology, A*STAR, for support with zebrafish experiments.

This work was supported by grants from the National Research Foundation, Ministry of Health, and Ministry of Education, Singapore (NRF-NRFI2017-05, MOH-000217, MOE-T2EP30220-0001, and MOE2019-T2-1-031 [D.L.S.] and NRF-NRFF2017-05 [L.H.]), a Goh Cardiovascular Research Award (D.L.S.), a grant from Howard Hughes Medical Institute International Research Scholar Program (HHMI-IRSP55008732 [L.H.]), and a grant from the Human Frontier Science Program (LT000733/2020-L [A.C.Y.K.]).

Author affiliations: [a]Signature Research Program in Cardiovascular and Metabolic Disorders, Duke-National University of Singapore (NUS) Medical School, 169857, Singapore; [b]Singapore Lipidomics Incubator, Life Sciences Institute, NUS, 117456, Singapore; [c]Department of Biochemistry, Yong Loo Lin School of Medicine, NUS, 117596, Singapore; [d]Institute of Molecular and Cell Biology, A*STAR, 138673, Singapore; and [e]Institute of Medical Biology, A*STAR, 138648, Singapore

Author contributions: M.H., A.C.Y.K., J.M.N., L.H., and D.L.S. designed research; M.H., A.C.Y.K., M.D., C.F.C., D.L.A.G., J.M.N., B.C.T., H.L.Y., and G.L.C. performed research; P.I.B., M.R.W., L.H., and F.T. contributed new reagents/analytic tools; M.H., A.C.Y.K., M.D., F.T., and D.L.S. analyzed data; and M.H. and D.L.S. wrote the paper.

1. F. M. Platt, A. d'Azzo, B. L. Davidson, E. F. Neufeld, C. J. Tifft, Lysosomal storage diseases. *Nat. Rev. Dis. Primers* **4**, 27 (2018).
2. V. Kalatzis, S. Cherqui, C. Antignac, B. Gasnier, Cystinosin, the protein defective in cystinosis, is a H(+)-driven lysosomal cystine transporter. *EMBO J.* **20**, 5940–5949 (2001).
3. P. Morin, C. Sagné, B. Gasnier, Functional characterization of wild-type and mutant human sialin. *EMBO J.* **23**, 4560–4570 (2004).
4. S. van Veen *et al.*, ATP13A2 deficiency disrupts lysosomal polyamine export. *Nature* **578**, 419–424 (2020).
5. R. E. Infante *et al.*, NPC2 facilitates bidirectional transfer of cholesterol between NPC1 and lipid bilayers, a step in cholesterol egress from lysosomes. *Proc. Natl. Acad. Sci. U.S.A.* **105**, 15287–15292 (2008).
6. E. Lloyd-Evans *et al.*, Niemann-Pick disease type C1 is a sphingosine storage disease that causes deregulation of lysosomal calcium. *Nat. Med.* **14**, 1247–1255 (2008).
7. G. Tettamanti, R. Bassi, P. Viani, L. Riboni, Salvage pathways in glycosphingolipid metabolism. *Biochimie* **85**, 423–437 (2003).
8. S. Lima, S. Milstien, S. Spiegel, Sphingosine and sphingosine kinase 1 involvement in endocytic membrane trafficking. *J. Biol. Chem.* **292**, 3074–3088 (2017).
9. S. Fowler, C. De Duve, Digestive activity of lysosomes. 3. The digestion of lipids by extracts of rat liver lysosomes. *J. Biol. Chem.* **244**, 471–481 (1969).
10. R. Franson, M. Waite, M. LaVia, Identification of phospholipase A 1 and A 2 in the soluble fraction of rat liver lysosomes. *Biochemistry* **10**, 1942–1946 (1971).
11. K. Y. Hostetler, P. J. Yazaki, H. van den Bosch, Purification of lysosomal phospholipase A. Evidence for multiple isoenzymes in rat liver. *J. Biol. Chem.* **257**, 13367–13373 (1982).
12. M. Hiraoka *et al.*, Lysosomal phospholipase A2 and phospholipidosis. *Mol. Cell. Biol.* **26**, 6139–6148 (2006).
13. W. E. Lands, Metabolism of glycerolipids. 2. The enzymatic acylation of lysolecithin. *J. Biol. Chem.* **235**, 2233–2237 (1960).
14. L. N. Nguyen *et al.*, Mfsd2a is a transporter for the essential omega-3 fatty acid docosahexaenoic acid. *Nature* **509**, 503–506 (2014).
15. R. J. Cater *et al.*, Structural basis of omega-3 fatty acid transport across the blood-brain barrier. *Nature* **595**, 315–319 (2021).
16. Y. Hisano, N. Kobayashi, A. Yamaguchi, T. Nishi, Mouse SPNS2 functions as a sphingosine-1-phosphate transporter in vascular endothelial cells. *PloS One* **7**, e38941 (2012).
17. T. M. Vu *et al.*, Mfsd2b is essential for the sphingosine-1-phosphate export in erythrocytes and platelets. *Nature* **550**, 524–528 (2017).
18. D. Q. Quek, L. N. Nguyen, H. Fan, D. L. Silver, Structural insights into the transport mechanism of the human sodium-dependent lysophosphatidylcholine transporter MFSD 2A. *J. Biol. Chem.* **291**, 9383–9394 (2016).
19. C. A. P. Wood *et al.*, Structure and mechanism of blood-brain-barrier lipid transporter MFSD2A. *Nature* **596**, 444–448 (2021).
20. C. D. Go *et al.*, A proximity-dependent biotinylation map of a human cell. *Nature* **595**, 120–124 (2021).
21. S. Ponnaiyan, F. Akter, J. Singh, D. Winter, Comprehensive draft of the mouse embryonic fibroblast lysosomal proteome by mass spectrometry based proteomics. *Sci. Data* **7**, 68 (2020).
22. T. Braulke, J. S. Bonifacino, Sorting of lysosomal proteins. *Biochim. Biophys. Acta* **1793**, 605–614 (2009).
23. S. Fukuhara *et al.*, The sphingosine-1-phosphate transporter Spns2 expressed on endothelial cells regulates lymphocyte trafficking in mice. *J. Clin. Invest.* **122**, 1416–1426 (2012).
24. Y. Rong *et al.*, Spinster is required for autophagic lysosome reformation and mTOR reactivation following starvation. *Proc. Natl. Acad. Sci. U.S.A.* **108**, 7826–7831 (2011).
25. T. Sasaki *et al.*, Autolysosome biogenesis and developmental senescence are regulated by both Spns1 and v-ATPase. *Autophagy* **13**, 386–403 (2017).
26. T. Sasaki *et al.*, Aberrant autolysosomal regulation is linked to the induction of embryonic senescence: Differential roles of Beclin 1 and p53 in vertebrate Spns1 deficiency. *PloS Genet.* **10**, e1004409 (2014).
27. D. M. Hatters, C. A. Peters-Libeu, K. H. Weisgraber, Apolipoprotein E structure: Insights into function. *Trends Biochem. Sci.* **31**, 445–454 (2006).
28. R. M. Young *et al.*, Zebrafish yolk-specific not really started (NRS) gene is a vertebrate homolog of the Drosophila spinster gene and is essential for embryogenesis. *Dev. Dyn.* **223**, 298–305 (2002).
29. L. Mach, K. Stüwe, A. Hagen, C. Ballaun, J. Glössl, Proteolytic processing and glycosylation of cathepsin B. The role of the primary structure of the latent precursor and of the carbohydrate moiety for cell-type-specific molecular forms of the enzyme. *Biochem. J.* **282**, 577–582 (1992).
30. A. K. Tharkeshwar *et al.*, A novel approach to analyze lysosomal dysfunctions through subcellular proteomics and lipidomics: The case of NPC1 deficiency. *Sci. Rep.* **7**, 41408 (2017).
31. H. Schulze, K. Sandhoff, Lysosomal lipid storage diseases. *Cold Spring Harb. Perspect. Biol.* **3**, a004804 (2011).
32. A. Ballabio, V. Gieselmann, Lysosomal disorders: From storage to cellular damage. *Biochim. Biophys. Acta* **1793**, 684–696 (2009).
33. B. Dermaut *et al.*, Aberrant lysosomal carbohydrate storage accompanies endocytic defects and neurodegeneration in Drosophila benchwarmer. *J. Cell Biol.* **170**, 127–139 (2005).
34. C. Dall'Armi, K. A. Devereaux, G. Di Paolo, The role of lipids in the control of autophagy. *Curr. Biol.* **23**, R33–R45 (2013).
35. L. V. Chernomordik, E. Leikina, V. Frolov, P. Bronk, J. Zimmerberg, An early stage of membrane fusion mediated by the low pH conformation of influenza hemagglutinin depends upon membrane lipids. *J. Cell Biol.* **136**, 81–93 (1997).
36. N. Fuller, R. P. Rand, The influence of lysolipids on the spontaneous curvature and bending elasticity of phospholipid membranes. *Biophys. J.* **81**, 243–254 (2001).
37. M. Flint *et al.*, A genome-wide CRISPR screen identifies N-acetylglucosamine-1-phosphate transferase as a potential antiviral target for Ebola virus. *Nat. Commun.* **10**, 285 (2019).
38. R. Wang *et al.*, Genetic screens identify host factors for SARS-CoV-2 and common cold coronaviruses. *Cell* **184**, 106–119 e114 (2021).
39. V. C. Hannah, J. Ou, A. Luong, J. L. Goldstein, M. S. Brown, Unsaturated fatty acids down-regulate srebp isoforms 1a and 1c by two mechanisms in HEK-293 cells. *J. Biol. Chem.* **276**, 4365–4372 (2001).
40. H. Liu, J. H. Naismith, An efficient one-step site-directed deletion, insertion, single and multiple-site plasmid mutagenesis protocol. *BMC Biotechnol.* **8**, 91 (2008).
41. J. Yang *et al.*, The I-TASSER Suite: Protein structure and function prediction. *Nat. Methods* **12**, 7–8 (2015).
42. J. Jumper *et al.*, Highly accurate protein structure prediction with AlphaFold. *Nature* **596**, 583–589 (2021).
43. D. G. Gibson *et al.*, Enzymatic assembly of DNA molecules up to several hundred kilobases. *Nat. Methods* **6**, 343–345 (2009).
44. M. Thelen, D. Winter, T. Braulke, V. Gieselmann, SILAC-based comparative proteomic analysis of lysosomes from mammalian cells using LC-MS/MS. *Methods Mol. Biol.* **1594**, 1–18 (2017).
45. B. H. Wong *et al.*, The lipid transporter Mfsd2a maintains pulmonary surfactant homeostasis. *J. Biol. Chem.* **298**, 101709 (2022).